Extended x-ray-absorption fine-structure measurements of copper: Local dynamics, anharmonicity, and thermal expansion

P. Fornasini,* S. a Beccara, G. Dalba, R. Grisenti, A. Sanson, and M. Vaccari
Istituto Nazionale per la Fisica della Materia and Dipartimento di Fisica, Università di Trento, I-38050 Povo (Trento), Italy

F. Rocca
IFN, Istituto di Fotonica e Nanotecnologie del Consiglio Nazionale delle Ricerche, Sezione CeFSA di Trento-38050 Povo (Trento), Italy

(Received 23 March 2004; revised manuscript received 17 June 2004; published 2 November 2004)

Extended x-ray-absorption fine-structure (EXAFS) of copper has been measured from 4 to 500 K and analyzed by the cumulant method, to check the effectiveness of EXAFS as a probe of local dynamics and thermal expansion. The comparison between parallel mean square relative displacements (MSRD) of the first four coordination shells has allowed detecting a significant deviation from a pure Debye behavior. The first-shell EXAFS thermal expansion is larger than the crystallographic one: the difference has allowed evaluating the perpendicular MSRD, whose Debye temperature is slightly larger than the one of the parallel MSRD, due to anisotropy effects. High-order first-shell cumulants are in good agreement with quantum perturbative models. The anharmonic contribution to the first-shell parallel MSRD amounts to less than 1.5 percent. The third cumulant cannot be neglected in the analysis, if accurate values of the first cumulant are sought; it cannot however be used to directly estimate the thermal expansion. The shape of the effective pair potential is independent of temperature; a rigid shift, partially due to the relative motion perpendicular to the bond direction, is however observed.

DOI: 10.1103/PhysRevB.70.174301 PACS number(s): 61.10.Ht, 65.40.−b

I. INTRODUCTION

Since the 1970s, extended x-ray-absorption fine structure (EXAFS) is considered a powerful probe of the local structure in various kinds of disordered systems.[1] A great theoretical effort has been made in the last years to calculate EXAFS spectra taking into account multiple scattering and curved wave effects.[2] A reliable and effective treatment of thermal and structural disorder still represents however an open problem, whose solution is expected to increase the amount and accuracy of information obtainable from EXAFS.

Thermal disorder has been frequently treated within the harmonic approximation, leading to a Gaussian distribution of interatomic distances, whose variance σ^2 corresponds to the mean square relative displacement (MSRD) $\langle \Delta u_{\parallel}^2 \rangle$ *parallel* to the bond between absorber and back-scatterer atoms.[3,4] The EXAFS Debye-Waller factor $\exp(-2\sigma^2 k^2)$ is often considered as a mere fitting parameter; only occasionally it has been exploited to gain information on the correlated motion of neighboring atoms.[5]

Anharmonicity effects on EXAFS have been detected quite early.[6] After the first pioneering studies on AgI (Ref. 7) and CuBr,[8] it has been shown that anharmonicity cannot be neglected even in systems like germanium[9] or GaAs.[10] Particularly effective, for treating anharmonicity in moderately disordered systems, is the cumulant expansion method,[11–14] which facilitates the experimental data analysis[8,15,16] as well as their theoretical interpretation.[17–21] The EXAFS cumulants parametrize the asymmetric distribution of interatomic distances, and can be connected to the force constants of a one-dimensional effective pair potential.[22,23] In particular, the first three cumulants measure the average value, the variance, and the asymmetry of the distribution, respectively.

EXAFS can be exploited to study the thermal expansion of selected interatomic distances. Both the first and third cumulants have often been considered equally sensitive to thermal expansion.[24] This equivalence, which is valid for a one-dimensional system, where the average distance is solely modified by the asymmetry of the interaction potential, was not confirmed by accurate EXAFS measurements of nearest-neighbors distances in several simple crystals.[6,25,26] Actually, the first EXAFS cumulant is larger than the distance between the centers of the probability distribution functions, owing to the effect of atomic vibrations perpendicular to the bond direction,[27,28] and its temperature dependence is stronger than the thermal expansion measured by Bragg diffraction or by macroscopic techniques. The difference between EXAFS and crystallographic thermal expansion can be exploited to gain original information on the MSRD $\langle \Delta u_{\perp}^2 \rangle$ *perpendicular* to the bond direction.[26] As far as the third cumulant is concerned, contradictory results were obtained for different crystals; the thermal expansion solely due to the asymmetry of the distribution, evaluated from the third cumulant, is smaller than the first-cumulant thermal expansion but equal to the crystallographic thermal expansion in the first coordination shell of germanium;[26] in AgI, CuBr, and CdSe, on the contrary, it is larger than the first-cumulant thermal expansion and non-negligbly different from the crystallographic thermal expansion.[25,29,30] A recent study of Ag_2O has demonstrated that accurate EXAFS measurements can give unique information on the local behavior of systems affected by negative thermal expansion.[31]

These results open new perspectives for EXAFS studies of the local dynamics in crystalline and noncrystalline mate-

rials. On the other hand, they pose also relevant questions about the very meaning of EXAFS cumulants in relation to physical properties of three-dimensional systems, the ultimate accuracy which can affect their determination, and the reliability and limitations of the one-dimensional model. The cumulant approach has been criticized on different grounds.[32,33] A reliable assessment of its strengths and limitations can only be based on careful experimental studies of systems of known structure and dynamical properties.

In this paper, we present an EXAFS study of Copper, in the temperature interval from 4–500 K. Copper has often been used as reference system for calibrating the procedures of EXAFS data analysis and the interpretation of results.[2,34–37] Main aim of the present study is to understand the extent and accuracy of information concerning thermal expansion and local dynamics obtainable from EXAFS. Some preliminary results for the first shell have been presented elsewhere, in a rapid communication dedicated to path-integral Monte Carlo calculations.[38]

Section II contains a synthetic and up-to-date introduction to the cumulant method, enlightening the most recent developments and emphasizing the differences between one-dimensional model and three-dimensional crystals. In Sec. III some experimental details are given on temperature dependent EXAFS measurements on copper. In Sec. IV the data analysis procedures are depicted. In Sec. V the results of EXAFS analysis are presented. Sections VI and VII are dedicated to a discussion of results and to conclusions, respectively.

II. THEORY

The effects of thermal disorder on the EXAFS signal of one given scattering path can be calculated from the canonical average of the oscillatory function:[39]

$$\left\langle \frac{e^{2ikr}e^{-2r/\lambda(k)}}{r^2} \right\rangle = \frac{\mathrm{Tr}\{e^{-\beta\hat{H}}e^{2ikr}e^{-2r/\lambda(k)}/r^2\}}{\mathrm{Tr}\{e^{-\beta\hat{H}}\}}, \tag{1}$$

where r is the instantaneous half-path-length (corresponding to the interatomic distance for single-scattering paths), k is the photoelectron wave number, $\lambda(k)$ is the photoelectron mean free path, and $\hat{H}$ is the system Hamiltonian.

For moderate disorder, the logarithm of the canonical average can be expanded as a power series of k,

$$\left\langle \frac{e^{2ikr}e^{-2r/\lambda(k)}}{r^2} \right\rangle = \exp\left[\sum_{n=0}^{\infty} (2ik)^n C_n \Big/ n! \right]. \tag{2}$$

The parameters C_n are the *cumulants* of an *effective distribution* $P(r,\lambda)=\rho(r)\exp(-2r/\lambda)/r^2$, where $\rho(r)$ is the *real distribution* of interatomic distances. Phase and amplitude of the EXAFS signal of a selected path can be parametrized in terms of odd and even cumulants, respectively.

The relations between cumulants of the *real* and *effective* distributions, C_n^* and C_n, respectively, as well as the effects of neglecting the k dependence of λ, have been discussed in Refs. 11 and 14. The first cumulants (average values) are connected through the relation

$$C_1 = C_1^* - \frac{2C_2^*}{C_1^*}\left(1 + \frac{C_1^*}{\lambda}\right), \tag{3}$$

which is customarily used. For higher order cumulants, the difference is less important,[14] and is generally neglected for moderate disorder.

A. One-dimensional model

The interpretation of EXAFS cumulants is simple for a one-dimensional system (like a two-atomic molecule, if rotational motion is neglected). The one-dimensional interatomic potential is conveniently expanded as a power series of the instantaneous displacement $x=r-r_0$ with respect to the minimum position r_0,

$$V(x) = k_0x^2/2 + k_3x^3 + k_4x^4 + \cdots, \tag{4}$$

where k_0 and $k_3, k_4, \ldots$ are the harmonic and higher order (anharmonic) force constants, respectively. The thermal expansion $\langle x\rangle = \langle r - r_0\rangle$ is due to the asymmetry of the potential.

A quantitative relation between EXAFS cumulants and force constants, based on a perturbative quantum approach,[40] has been proposed by Frenkel and Rehr[17] and extended by Yokoyama.[23] Let us recall here some relevant results. Considering the harmonic term of the potential as unperturbed Hamiltonian, and defining

$$\omega = \sqrt{k_0/\mu}, \quad \sigma_0^2 = \hbar/2\mu\omega, \quad z = e^{-\beta\hbar\omega} \tag{5}$$

(μ is the reduced mass) one can find the following first order expressions. The temperature dependence of the first cumulant $\delta C_1^* = \langle x\rangle$ is

$$\delta C_1^* \simeq -\frac{3k_3\sigma_0^2}{k_0}\frac{1+z}{1-z}. \tag{6}$$

The second cumulant in harmonic approximation is

$$C_2 \simeq \sigma_0^2\frac{1+z}{1-z}; \tag{7}$$

higher order anharmonic terms are also given in Ref. 23 [where, in the second term of Eq. (12), a factor 120 should be substituted for 24].[41] The third cumulant is

$$C_3^* \simeq -\frac{2k_3\sigma_0^4}{k_0}\frac{z^2+10z+1}{(1-z)^2}. \tag{8}$$

The thermal expansion

$$\langle x\rangle \simeq \delta C_1^* \simeq -\frac{3k_3}{k_0}C_2^* \tag{9}$$

can be equivalently obtained from the temperature dependence of the first cumulant or of the second and third cumulants. In the classical approximation[24]

$$\delta C_1^* = C_3^*/2C_2^*, \tag{10}$$

which is equivalent to Eq. (9) only in the high-temperature limit.

An experimental EXAFS study of the anharmonic interatomic potential in the Br_2 molecule has been recently done by Yokoyama *et al.*[42]

B. Crystals

In crystals, an EXAFS spectrum still samples a one-dimensional distribution of distances for each scattering path, but now the potential is defined within a $3N$-dimensional configurational space, N being the number of atoms. The interpretation of EXAFS cumulants thus requires a specific treatment.

Let us define a distance R_0, between a pair of absorber and back-scatterer atoms, corresponding to an ideal classical state of absolute rest. When thermal disorder is switched on (including zero point motion), the instantaneous relative thermal displacement of absorber and back-scatterer atoms, $\Delta\vec{u} = \vec{u}_j - \vec{u}_0$, can be decomposed into its projections $\Delta u_\parallel$ and $\Delta u_\perp$ along the average bond direction and in the perpendicular plane, respectively. The instantaneous interatomic distance is, to first approximation,[13]

$$r \simeq R_0 + \Delta u_\parallel + \Delta u_\perp^2/2R_0. \tag{11}$$

Within the framework of a quasiharmonic approach, the parallel relative displacement of Eq. (11) can be decomposed into a harmonic and an anharmonic contribution,

$$\Delta u_\parallel = (\Delta u_\parallel)_h + (\Delta u_\parallel)_{\mathrm{an}}. \tag{12}$$

Let us now consider canonical averages. The three-dimensional distribution of relative distances being an ellipsoid in the harmonic approximation, $\langle \Delta u_\parallel \rangle_h = 0$, and the first EXAFS cumulant $C_1^* = \langle r \rangle$ is

$$C_1^* \simeq R_0 + \langle \Delta u_\parallel \rangle_{\mathrm{an}} + \langle \Delta u_\perp^2 \rangle / 2R_0, \tag{13}$$

while the crystallographic distance R_c between the centroids of the probability distribution functions, measured by Bragg diffraction, is

$$R_c = R_0 + \langle \Delta u_\parallel \rangle_{\mathrm{an}}. \tag{14}$$

Both $\langle \Delta u_\parallel \rangle_{\mathrm{an}}$ and $\langle \Delta u_\perp^2 \rangle$ have finite values at zero kelvin, due to the zero point motion.

The average distance measured by EXAFS is larger than the crystallographic distance,

$$C_1^* \simeq R_c + \langle \Delta u_\perp^2 \rangle / 2R_0. \tag{15}$$

Since $\langle \Delta u_\perp^2 \rangle$ depends on temperature, also the thermal expansion δC_1^* measured by EXAFS is larger than the crystallographic thermal expansion δR_c. This effect is of geometrical origin, and would be present also for a perfectly harmonic crystal.[14]

The second cumulant is $C_2^* = \langle (r - \langle r \rangle)^2 \rangle$. Expanding Eq. (11), one can show that in the harmonic approximation

$$C_2^* \simeq \langle \Delta u_\parallel^2 \rangle - \frac{\langle \Delta u_\parallel^2 \Delta u_\perp^2 \rangle}{R_0^2} + \frac{[\langle \Delta u_\perp^4 \rangle - \langle \Delta u_\perp^2 \rangle^2]}{4R_0^2}, \tag{16}$$

where the first term on the right-hand side is the parallel MSRD, and the third term is the variance of the distribution of $\Delta u_\perp^2$. It is customary to truncate Eq. (16) at the first leading term,

$$C_2^* \simeq \langle \Delta u_\parallel^2 \rangle, \tag{17}$$

and to fit its temperature dependence to phenomenological models (correlated Debye and Einstein models). The parallel MSRD can in turn be decomposed[3] into the sum of the uncorrelated mean square displacements (MSD) of absorber and back-scatterer atoms and of the displacement correlation function (DCF).

The third cumulant $C_3^* = \langle (r - \langle r \rangle)^3 \rangle$ measures the asymmetry of the distribution of distances, which is mainly due to the anharmonicity of the crystal potential.[14]

The interpretation of EXAFS cumulants for crystals is often carried on with reference to a one-dimensional *effective potential*, which is expanded as in Eq. (4). The effective pair potential depends however on the statistically averaged behavior of all the atoms in the crystal, and is in principle temperature dependent, both in position and shape. One can show that the temperature dependence of $\langle \Delta u_\perp^2 \rangle$ corresponds to a positive shift of the minimum of the effective pair potential.[14] The EXAFS thermal expansion δC_1^* thus depends not only on the asymmetry of the effective potential, like for the one-dimensional case, but also on its rigid shift, which originates from thermal vibrations perpendicular to the bond direction and possibly from other causes.[25,29,30] Accordingly, Eq. (6) and (9) are not valid for many-dimensional systems. The quantities δC_1^* and $a = -3k_3 C_2^*/k_0$ are not equivalent in crystals. To the extent that the shape of the effective potential is independent of temperature, Eqs. (7) and (8) are instead still valid. Equation (7) corresponds to the Einstein correlated model, and the Einstein frequency allows measuring an *effective* bond-stretching force constant k_0.

When considering multiple scattering (MS) paths, one frequently indicates by r the *total* path length, so that first and second cumulants are expressed as

$$C_1^* = \langle r \rangle / 2, \quad C_2^* = \langle (r - \langle r \rangle)^2 \rangle / 4. \tag{18}$$

Generalizing Eq. (13) gives

$$\langle r \rangle \simeq R_0 + \sum_{i=1}^{n} \langle \Delta u_\parallel \rangle_{\mathrm{an}}^{i,i+} + \sum_{i=1}^{n} \frac{\langle \Delta u_\perp^2 \rangle^{i,i+}}{2R_0^{i,i+}}, \tag{19}$$

where R_0 is now the total frozen path length, the sums are over the path lengths, and $i+$ is a short-hand notation for $i+1$ (but $n+=1$). Similarly, generalizing Eq. (17) gives[2]

$$\langle (r - \langle r \rangle)^2 \rangle \simeq \left\langle \left| \sum_{i=1}^{n} (\vec{u}_{i+} - \vec{u}_i) \cdot \hat{R}_0^{i,i+} \right|^2 \right\rangle. \tag{20}$$

III. EXPERIMENT

The available experimental EXAFS data on copper mainly date back to early pioneering experiments, and are anyway limited to a few temperatures.[34–37] In order to deal with high-quality spectra, reasonably distributed within a large temperature interval, new measurements have been made with synchrotron radiation at the BM08 (Gilda) beamline of ESRF (European Synchrotron Radiation Facility) in Grenoble (France). Electron energy and average current were

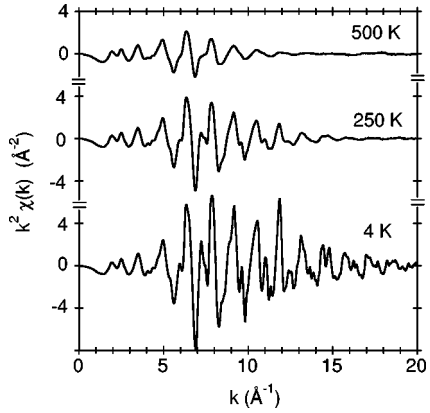

FIG. 1. Normalized EXAFS oscillations $k^2\chi(k)$ at the K edge of copper, measured at 4, 250, and 500 K.

6 GeV and 190 mA, respectively. The sample was a copper foil of 99.97% purity, 5 μm thickness, light tested and annealed at 973 K (purchased from Goodfellow Ltd.).

The x-ray beam was monochromatized by two parallel silicon crystals with flat reflecting (311) faces, detuned to reduce the harmonics influence. The beam intensity was measured before and past the sample by two argon-filled ionization chambers. The sample temperature was varied from 4 to 500 K, at intervals varying from 5 K at low temperatures to 50 K at high temperatures. At and below 300 K, a liquid helium cryostat was utilized, where the sample was immersed in a He gas athmosphere; at and above 300 K, the sample was maintained in thermal contact with the cold finger of a liquid nitrogen cryostat. In both cases, a preset temperature was maintained by means of an electric heater controlled by a feedback loop. The temperature, directly measured on the sample holder, was stabilized to an accuracy not worse than 0.5 K. The acquisition time was 5 s/point. Two or three spectra were measured at some selected temperatures, to allow an evaluation of experimental uncertainty. The value of the absorption jump at the Cu K edge was $\mu x \simeq 1.2$, and did not vary by more than 2 percent during the entire experiment.

IV. DATA ANALYSIS

At the beginning of the analysis, the edges of all spectra were aligned to within 0.1 eV or better. The EXAFS signal was obtained as $\chi(k)=[\mu(k)-\mu_1(k)]/\mu_0(k)$, where $\mu(k)$ is the experimental absorption coefficient, $\mu_1(k)$ is a spline polynomial best fitting the average behavior of $\mu(k)$, and $\mu_0(k)$ is a smooth Victoreen-type function ($\propto\lambda^{2.8}$, where λ is here the photon wavelength) with absolute values normalized to the absorption jump of each spectrum. The EXAFS oscillations at selected temperatures are shown in Fig. 1.

The corresponding Fourier transforms are shown in Fig. 2. The first-shell peak, centered at about 2.3 Å, is well isolated at all temperatures. It was then possible to single out the first-shell contribution by Fourier back-transform. The structure between about 3 and 5.3 Å formed by three peaks which are well separated at 4 K but progressively merge

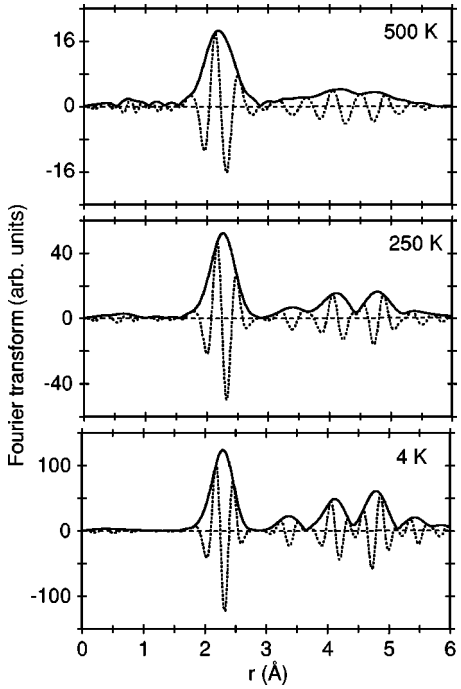

FIG. 2. Fourier transforms of the EXAFS signal of copper at 4, 250, and 500 K. Continuous and dotted lines are the modulus and the imaginary part, respectively. The transforms have been made in the interval $k=2$–20 Å^{-1}, with a k^3 weighting and a 10% Gaussian window for all three spectra.

when temperature increases, is due to the superposition of single scattering (SS) contributions from second, third, and fourth shells as well as of rather important MS contributions.[2] Two different procedures were then utilized to obtain quantitative information.

The *first procedure* was utilized only for the first coordination shell, whose contribution could be neatly isolated, and where MS effects were absent. It consisted in the separate analysis of phase and amplitude of the filtered EXAFS signal through the *ratio method*,[11,14] taking the lowest temperature spectra as reference for backscattering amplitudes, phase shifts, and inelastic terms. In Fig. 3, phase differences and logarithms of amplitude ratios for the first coordination shell of copper are plotted against k^2 for selected temperatures. The subscripts 1 and 2 indicate the reference (4 K) and the actual temperature, respectively. In the plot of $(\Phi_2-\Phi_1)/2k$ (Fig. 3, upper panel), the vertical intercept is δC_1 while the linear slope is proportional to the third cumulant variation δC_3. In the plot of $\ln(A_2/A_1)$ (Fig. 3, lower panel) the linear slope is proportional to the variation of the second cumulant δC_2. The *ratio method*, when applicable, allows a visual estimate of the overall quality of experimental data and of the useful k range, which typically decreases when temperature increases. The error on interatomic distances deriving from neglecting the third cumulant is evident, and the deviation from linear behavior indicates the possible relevance of higher order cumulants. Actually, since the cumulant series of Eq. (2) was truncated at the fourth-order term, the results of the analysis were the relative values of four polynomial coefficients $\delta\tilde{C}_n=\tilde{C}_n(T)-\tilde{C}_n(4K)$. The good correspondence

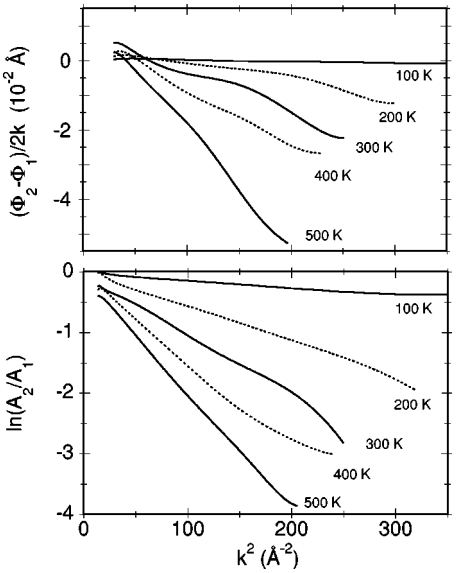

FIG. 3. First shell of copper, examples of analysis by the ratio method at selected temperatures. Upper panel, phase differences. Lower panel, logarithms of amplitude ratios.

of the polynomial coefficients with the cumulants C_n of the *effective* distribution of distances $P(r,\lambda)$ was *a posteriori* checked by the regular temperature dependence of their values (see below).[14,26]

In the *second procedure*, EXAFS spectra were simulated at different temperatures by the FEFF8 code,[43] and the cumulant values were obtained through a nonlinear best-fit to experimental spectra (the FEFFIT code[44] was utilized to this purpose). In principle this procedure (in the following referred to as *theoretical*) should give absolute values of cumulants; actually, significant absolute values with an accuracy sufficient for the aims of this work were obtained only for the second cumulant; relative values were then considered for the other cumulants. For the first-shell analysis, the theoretical procedure was used to check the results of the ratio method. For the outer shells, it represented the only reasonable way for taking into account both SS and MS contributions between 3 and 5.3 Å in the Fourier transformed spectrum of Fig. 2. A particular care was devoted to reducing as much as possible the number of free parameters. Let us here consider E_0, the edge energy mismatch between theory and experiment, and S_0^2, the amplitude reduction factor taking into account intrinsic inelastic effects.[2] The values of E_0 and S_0^2, left free in a first trial analysis, varied as a function of temperature (typically, $E_0 \simeq 2.8$–4 eV, $S_0^2 \simeq 0.84$–0.88 for the first shell). Average values were then calculated ($E_0 = 3.19$ eV, $S_0^2 = 0.86$ for the first shell) and maintained fixed in a further analysis, leading to a substantial reduction of the uncertainty bars and of the scattering of cumulant values as a function of temperature.

V. RESULTS

A. First coordination shell

The relative values of the first three cumulants of the first coordination shell, obtained by the *ratio method*, are listed in Table I. The uncertainties, expressed as standard deviations

TABLE I. Temperature dependence of the EXAFS cumulants of the first coordination shell of copper, obtained by the *ratio method*. C_1 is the first cumulant of the effective distribution. C_1^* is the first cumulant of the real distribution, calculated for a constant mean free path $\lambda = 9$ Å.

T (K)	δC_1 (10^{-3} Å)	δC_1^* (10^{-3} Å)	δC_2^* (10^{-3} Å^2)	δC_3^* (10^{-4} Å^3)
10	0.0±0.4	0.0±0.4	0.00±0.01	0.00±0.03
15	0.1±0.3	0.1±0.3	0.02±0.01	0.00±0.03
20	0.0±0.3	0.0±0.3	0.01±0.01	0.00±0.03
25	0.0±0.3	0.0±0.3	0.00±0.01	0.01±0.03
40	0.0±0.3	0.0±0.3	0.03±0.01	0.01±0.03
55	0.1±0.3	0.3±0.3	0.18±0.01	0.02±0.03
70	−0.1±0.3	0.3±0.3	0.33±0.01	0.00±0.04
85	0.2±0.3	0.7±0.3	0.49±0.01	0.01±0.04
100	0.4±0.3	1.1±0.3	0.73±0.01	0.05±0.03
125	1.0±0.4	2.2±0.4	1.19±0.01	0.14±0.05
150	1.4±0.3	3.1±0.3	1.66±0.01	0.23±0.04
200	2.8±0.4	5.5±0.4	2.77±0.02	0.52±0.05
250	4.1±0.3	8.2±0.3	4.04±0.03	0.92±0.04
300	5.5±0.9	10.9±0.9	5.34±0.03	1.41±0.07
350	7.1±1.4	13.8±1.4	6.60±0.06	2.03±0.13
400	8.9±1.8	16.9±1.8	7.94±0.09	2.76±0.16
450	10.6±1.2	20.0±1.2	9.40±0.16	3.76±0.10
500	12.9±1.0	23.7±1.0	10.77±0.06	4.86±0.09

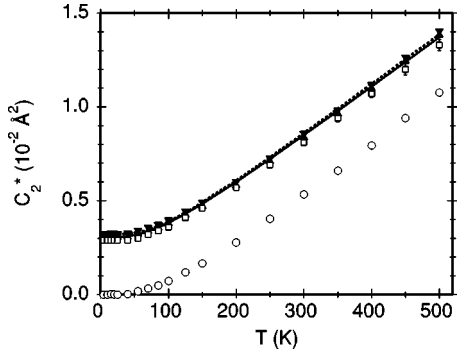

FIG. 4. First shell of copper, second cumulant, relative values from the *ratio method* (open circles, larger than uncertainty bars) and absolute values obtained through correlated Einstein and Debye models (down and up triangles, respectively). The dotted and continuous lines are the best fitting Einstein and Debye models, respectively. The squares are the absolute values obtained by a best fit to FEFF simulations.

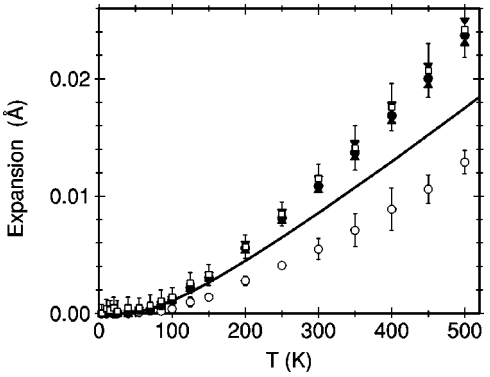

FIG. 5. First shell of copper, temperature variation of the first cumulant of the effective distribution (open circles) and of the real distribution (down triangles, full circles and up triangles for mean free path 6, 9, and 12 Å, respectively), obtained by the *ratio method*. The squares are the values obtained by a best fit to FEFF simulations. The continuous line is the crystallographic thermal expansion. The uncertainty bars are shown only for the open circles and the squares.

of the means, were evaluated by reasonably varying the parameters of the analysis procedure (Fourier transform window, and fitting intervals for differences of phases and amplitudes ratios) as well as cross comparing the results from different files measured at the same temperature. The refinement of the analysis allowed increasing the accuracy of cumulant values with respect to the preliminary presentation of Ref. 38.

The difference between cumulants C_i and C_i^* of the effective and real distributions, respectively, was significant only for the first cumulant,[14] to which Eq. (3) was applied. For higher order cumulants, after having checked the negligibility of the difference, we set $C_n^*=C_n$.

1. Second cumulant

It is convenient to begin the presentation of results from the second cumulant (Fig. 4). The *ratio method* (open circles) gives only relative values δC_2^*. Absolute values, corresponding to the parallel MSRD, were estimated by fitting Einstein and Debye correlated models[5] to the experimental δC_2^* data. The Einstein frequency was (4.96 ± 0.05) THz, corresponding to a second order effective force constant $k_0=3.20$ eV/Å^2. The Debye temperature was (328 ± 3) K. The Einstein model gave absolute values 1.2×10^{-4} Å^2 higher than the Debye model.

Absolute C_2^* values have been directly obtained from the theoretical analysis procedure. Their temperature dependence is consistent with an Einstein frequency of 4.96 THz; the values are however slightly lower than expected according to the Einstein model (from 3 to 7×10^{-4} Å^2 when going from 4 to 500 K).

2. First cumulant

Let us now consider the first cumulant (Fig. 5). The *ratio method* directly gives the relative values δC_1 for the *effective* distribution (open circles). The analysis procedure, based on the difference between total phases, cancels to a good approximation the k-dependent photoelectron mean free path $\lambda(k)$.[11,14] Relative values δC_1^* for the *real* distribution were sought through Eq. (3), making use of the experimental δC_2^* values. The k dependence of λ, in principle not negligible, cannot be analytically taken into account in this procedure. We thus calculated δC_1^* for three constant values of λ (6, 9, and 12 Å, respectively), and considered the spread of δC_1^* values as a reasonable measure of the uncertainty due to neglecting the k dependence.

Within this uncertainty, a good agreement is found with the relative δC_1^* values determined by the theoretical analysis. It should be noted that the theoretical procedure calculates the k dependence of $\lambda(k)$ from the imaginary part of the interaction potential, and uses a simplified form of Eq. (3), lacking the C_1^*/λ term.

As expected (Sec. II), the thermal expansion δC_1^* measured by EXAFS is larger than the crystallographic thermal expansion δR (continuous line in Fig. 5, calculated from Ref. 45), owing to the effect of the perpendicular MSRD. By inverting Eq. (15), relative values of $C_\perp=\langle\Delta u_\perp^2\rangle$ were obtained,

$$\delta C_\perp = 2R(\delta C_1^* - \delta R). \tag{21}$$

Absolute values of $\langle\Delta u_\perp^2\rangle$ were evaluated by fitting the $\delta C_\perp$ values to specifically tailored Debye or Einstein models, whose analytical expressions were found to correspond to the models for the parallel MSRD multiplied by a factor of 2 (this is intuitively understandable since $\Delta u_\perp$ is a projection into a plane instead of along a direction). The perpendicular MSRD values so obtained are shown in Fig. 6. No significant difference was found between the Debye and Einstein models. The correspondence between experimental points and theoretical models is not as good as for the parallel MSRD, particularly at high temperature. Besides reflecting the influence of larger uncertainty bars, this could also be due to stronger anharmonicity effects. The Debye temperatures corresponding to different values of the mean free path λ are

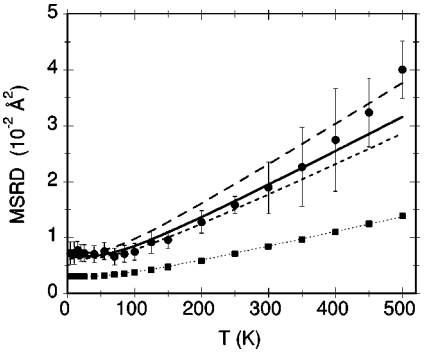

FIG. 6. Perpendicular MSRD for the first shell of copper, evaluated for a photoelectron mean free path of 9 Å (full circles). The long-dashed, continuous and short-dashed lines are the best fitting Debye models for photoelectron mean free paths of 6, 9, and 12 Å, respectively. The squares and the dotted line are the parallel MSRD and the best fitting Debye model, respectively.

shown in Table II. The spread of values can be considered a rough measure of their uncertainty. They are anyway larger than the corresponding values for the parallel MSRD, the gap decreasing when λ increases.

3. Third and fourth cumulants

Let us now consider the third cumulant (Fig. 7, upper panel), carrying on its interpretation within the framework of the one-dimensional model. The relative values δC_3^* obtained by both the ratio method and the theoretical analysis were in good agreement. Absolute values of C_3^* were obtained by fitting the temperature dependence of the values δC_3^* to Eq. (8). Using the second order force constant $k_0=3.20$ eV/Å^2 from the second cumulant analysis, the best fit was found for a third order force constant $k_3=-1.37$ eV/Å^3. The zero kelvin value was $C_3 \simeq 1\times10^{-5}$ Å^3.

The thermal expansion solely due to the asymmetry of the effective potential is, according to Eq. (9), $a=-3k_3C_2^*/k_0$.[17] Its relative values δa, based on the present EXAFS results, are shown in Fig. 7 (lower panel). As generally expected in crystals, δa is different from δC_1^* (Fig. 5). Besides, $\delta a(T)$ is different also from $\delta R(T)$, indicating that the crystallographic thermal expansion is not reproduced by the anharmonicity of the effective EXAFS potential. The behavior previously found for germanium, $\delta a \simeq \delta R$,[26] must then be considered as a peculiar coincidence, and cannot be generalized.

At last, let us consider the fourth cumulant (Fig. 8). The temperature dependence of the experimental δC_4^* values was fitted to the quantum analytical expression of Ref. 23 [where,

TABLE II. Einstein frequencies ν_1 and Debye temperatures θ_1 best fitting the temperature dependence of the parallel and perpendicular MSRDs of the first shell of copper.

	$\text{MSRD}_\perp$			$\text{MSRD}_\parallel$
	λ=6 Å	λ=9 Å	λ=12 Å	
ν_1 (THz)	4.19	4.57	4.81	4.96
θ_1 (K)	275	301	316	328

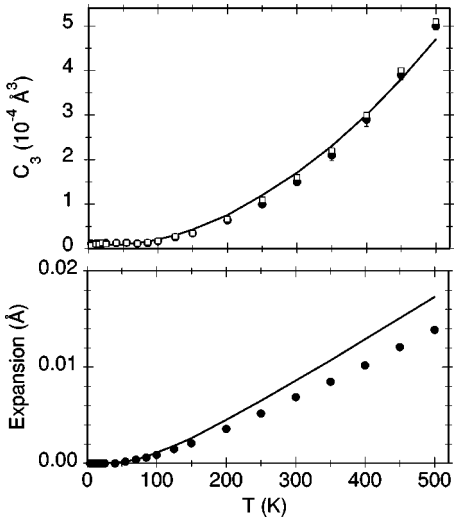

FIG. 7. Third cumulant (upper panel), absolute experimental values from ratio method (circles) and from theoretical procedure (squares); the continuous line is the best fitting theoretical model. Thermal expansion due to the asymmetry of the effective potential (lower panel, full circles; the continuous line is the crystallographic thermal expansion).

in the first term of Eq. (15), the factor $(\hbar\omega)^2$ in the denominator should be replaced by $\hbar\omega$].[41] The agreement is reasonably good. By imposing the values of second and third order force constants k_0 and k_3 previously obtained, the best fit was found for a fourth order force constant $k_4=1.46$ eV/Å^4. The zero kelvin value was $C_4 \simeq 4\times10^{-7}$ Å^4.

The knowledge of the third- and fourth-order force constants allowed estimating the anharmonic contribution to the second cumulant, using the high order corrections to Eq. (7) given in Ref. 23. The best fit was obtained by a tiny increase of the Einstein frequency (from 4.96 to 4.99 THz). The anharmonic correction resulted positive and very small (less than 1.5%).

B. Outer coordination shells

The analysis of the second, third, and fourth coordination shells was globally performed by the theoretical procedure, including all MS paths with relative importance larger than 2.5 percent with respect to the first-shell signal, and fitting the simulated spectra to the experimental ones in the *r*-space

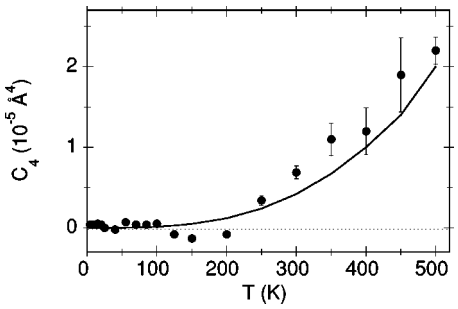

FIG. 8. Fourth cumulant, absolute experimental values (circles) and best fitting theoretical model (continuous line).

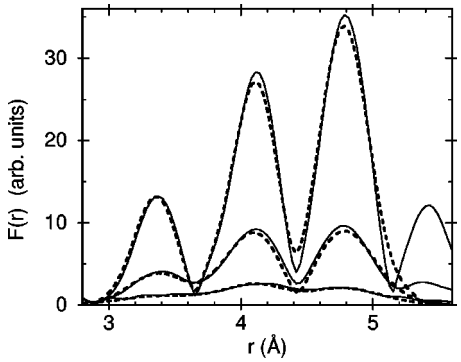

FIG. 9. Amplitude of Fourier transform of the experimental signals at 4, 250, and 500 K (continuous lines) and best fitting simulated signals (dashed lines).

between 2.9 and 5.25 Å. After a large number of trials, a reasonable agreement between theory and experiment (Fig. 9) could be obtained only by a drastic reduction of the fitting parameters, according to the following prescriptions: (a) the relative thermal expansion of all SS and MS paths was described by a unique fitting coefficient α; (b) the second cumulants of the three SS paths were considered as free parameters; (c) the second cumulants of the linear MS paths were linked to the second cumulants of SS paths by geometrical considerations, while the second cumulants of nonlinear MS paths were constrained to a Debye model with $\theta_D = 315$ K (average specific heat Debye temperature); (d) third and fourth cumulants were neglected for all paths.

The second cumulants (parallel MSRDs) of the SS paths are shown in Fig. 10. The comparison with the MSD measured by diffraction of Mössbauer gamma rays[47,48] allows evaluating the effect of correlation on the different coordination shells. The Debye temperatures were evaluated by fitting the Debye correlated model to experimental data in two different ranges, from 4 to 300 K and from 4 to 500 K, respectively, in order to check the effects of anharmonicity. First, third, and fourth shells share a very similar Debye temperature, independent of the fitting range (Table III); the second shell has instead a significantly lower Debye temperature,

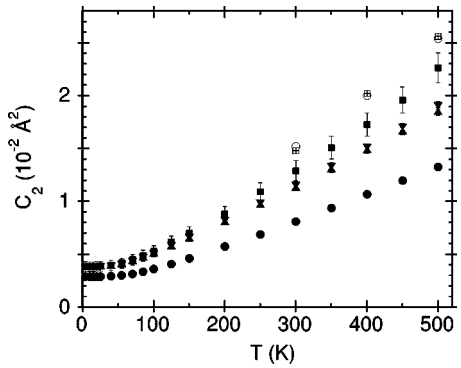

FIG. 10. Second EXAFS cumulant (parallel MSRD) of copper, first (full circles), second (full squares), third (up triangles), and fourth (down triangles) coordination shells. Open circles and crossed squares correspond to twice the uncorrelated MSDs from Refs. 47 and 48, respectively.

TABLE III. Debye temperatures (in K) of the parallel MSRDs of the first four shells of copper, for two different fitting intervals.

Fitting range	First shell	Second shell	Third shell	Fourth shell
4–300 K	328.5	291	322.5	322
4–500 K	328	283	322	321

whose dependence on the fitting range suggests a stronger sensitivity to anharmonicity. The MSRD values obtained from EXAFS are consistent, at high temperatures, with the ones recently calculated by means of molecular dynamics simulations.[46]

The average relative thermal expansion obtained through the best-fit procedure is compared in Fig. 11 with the crystallographic one. The good agreement should not be overemphasized; the thermal expansion calculated through molecular dynamics simulations[46] is larger than the crystallographic one also for the outer shells. The difference can be attributed to perpendicular thermal vibrations, although the effect is weaker than for the first shell. The present EXAFS analysis is insensitive to this difference probably as a consequence of neglecting the third cumulant. All attempts aiming at increasing the information quality and quantity from EXAFS were unsuccessful. In particular, the inclusion of the third cumulant in the signal of at least one of the coordination shells led to a prohibitively large correlation between first and third cumulant, which spoiled the results of any reasonable meaning.

VI. DISCUSSION

Three different logical steps have been singled out in the procedure of data analysis. In the first step, two three-dimensional distributions of atomic positions are reduced to the one-dimensional *real distribution* of interatomic distances, characterized by the cumulants C_n^*. This process, of geometrical nature, depends on the vibrational properties of the crystal. In the second step, the real distribution is sampled by the photoelectron spherical wave, leading to an *effective distribution* with cumulants C_n. This process depends on the EXAFS mechanism. The third step consists in

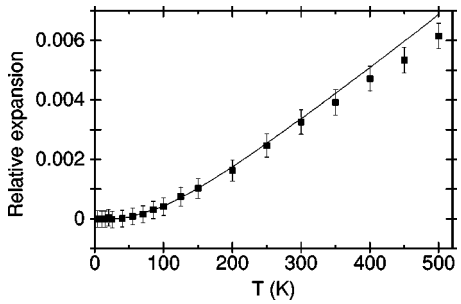

FIG. 11. Average relative thermal expansion best fitting the EXAFS signal corresponding to the second, third, and fourth coordination shells (squares). The continuous line is the crystallographic relative thermal expansion.

the extraction of a limited number of polynomial coefficients $\tilde{C}_n$ from EXAFS spectra.

The regular temperature dependence of the polynomial coefficients $\tilde{C}_n$, in agreement with theoretical expectations (Figs. 4, 5, 7, and 8), supports the hypothesis of a fast convergence of the cumulants series, and authorizes considering the polynomial coefficients as good estimates of the cumulants C_n. This self-consistent procedure is particularly suitable for evaluating the soundness of phenomenological analyses.[15] A further support to the fast convergence has been given by the reproduction of the first-shell EXAFS cumulants by path-integral Monte Carlo calculations.[38]

The distinction between real and effective distributions allows separating effects which depend on different physical causes, and can facilitate the comparison of EXAFS results with the results from other techniques.

A. Thermal expansion

Relevant information on thermal expansion (as well as on third and fourth cumulants) was obtained only for the first coordination shell.

Bragg diffraction measures the variation of the distance between the average atomic positions, which corresponds, for relatively simple crystals, to the thermal expansion measured by macroscopic dilatometry techniques. EXAFS measures the variation of the average value of the interatomic distance. The difference can be detected, at least in concentrated samples, by good quality transmission measurements (Fig. 5), and cannot be neglected in acurate works. Its origin is connected with the different sensitivity to local correlation of atomic motion. In this respect, thermal diffuse scattering (TDS) in Bragg diffraction spectra and x-ray or neutron scattering from noncrystalline materials contain in principle the same kind of information. EXAFS is however recommended for the relative easiness of temperature dependent measurements and accuracy attainable in data analysis.

The connection between first cumulants of the effective and real distributions [Eq. (3)] requires the knowledge of the parallel MSRD, which can be directly obtained from EXAFS. The connection between the distances measured by EXAFS and diffraction [Eq. (15)] requires the knowledge of the perpendicular MSRD, which cannot be evaluated solely from EXAFS. Actually, the relation between the parallel and perpendicular MSRD depends on the peculiar dynamical properties of a given crystal. As a matter of fact, in copper δC_1 is smaller and δC_1^* is larger than δR, while in germanium[26] both δC_1 and δC_1^* are larger than δR. The distance between the centroids of the probability distribution functions, as measured by Bragg diffraction, cannot be directly obtained from EXAFS, nor from other techniques similarly sensitive to local correlation.

The difference in thermal expansion values measured by EXAFS and Bragg diffraction can be positively exploited when investigating on the local origin of some anomalous dynamical behaviors, like negative thermal expansion (NTE). In many systems, NTE has been explained in terms of geometrical effects induced by low-frequency vibrational modes. In simple crystals with the diamond or zinc-blende structure (like germanium or GaAs), NTE is attributed to transverse acoustic modes which induce a guitar string effect.[49] In framework structures, composed of networks of corner-sharing tetrahedral and/or octahedral structural units, NTE has been attributed to the effect of rigid unit modes (RUM).[50] The sensitivity of EXAFS to the real thermal expansion of selected interatomic bonds and to the correlation of relative motion perpendicular to the bond represents a powerful tool for studying the local behavior of NTE materials and checking the soundness of theoretical models.[31] In this respect, EXAFS can be more accurate and experimentally simpler than the alternative approaches based on the analysis of TDS in total scattering experiments.[51]

Once the absolute values of the perpendicular MSRD have been evaluated, from the difference of EXAFS and diffraction thermal expansions and the fit to Debye or Einstein models, it is possible to recover the difference between the EXAFS and diffraction absolute distances, C_1^* and R_c, respectively. In the case of copper, taking into account the considered spread of mean free path values, the difference has been evaluated as $(1.4\pm0.1)\times10^{-3}$ Å at 4 K and $(3.9\pm0.4)\times10^{-3}$ Å at 300 K. Larger differences can be found in systems characterized by larger values of the perpendicular MSRD.

B. Mean square relative displacements

Both parallel and perpendicular MSRD carry original and independent information on the phase relationships between eigenvectors of the dynamical matrix. Their knowledge can be exploited to check the soundness of *ab initio* calculations as well as of dynamical models of different degrees of approximation.

The Debye temperatures best fitting the parallel MSRD of the first four coordination shells (Table III) can be compared with the Debye temperatures of specific heat ($\theta_D=345$ and 310 K at $T=0$ and 298 K, respectively) and of x-ray diffraction ($\theta_M=307$ and 327 K from the Bragg peaks intensities and from TDS, respectively),[52] as well as of more recent Mössbauer diffraction measurements (312 K).[48] Slight differences are expected between Debye temperatures measured by different techniques and in different conditions, in view of the different weightings of the density of vibrational states. In a perfect Debye crystal, the MSRDs of all coordination shells should be described by the same Debye temperature; the significantly lower value found for the second shell of copper indicates a weaker correlation effect for the next-nearest-neighbors distance, and suggests that also in close packed cubic crystals a slight vibrational anisotropy is present. Recently, a reduced correlation along the $\langle100\rangle$ direction was found in several fcc crystals by both dynamical calculations and pair distribution function measurements.[53]

The Debye temperature of the first-shell perpendicular MSRD is slightly lower than the one of the parallel MSRD (Table II). On general grounds, the difference between parallel and perpendicular MSRD depends on the peculiar dynamical properties of the crystal, and can be summarized by the temperature dependence of the ratio $\gamma=\langle\Delta u_\perp^2\rangle/\langle\Delta u_\parallel^2\rangle$. For an ideal Debye crystal, both parallel and perpendicular

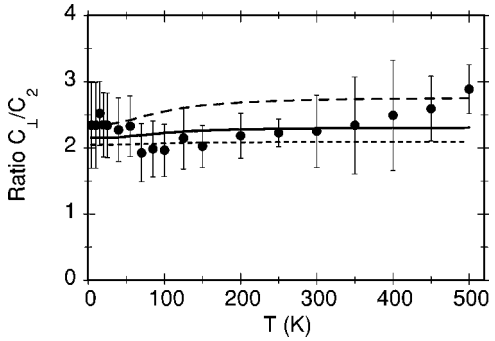

FIG. 12. Ratio $\langle \Delta u_\perp^2 \rangle / \langle \Delta u_\parallel^2 \rangle$ for $\lambda = 9$ Å (circles). The long dashed, continuous and short-dashed lines are the ratios of the best fitting Debye models for $\lambda = 6, 9, 12$ Å, respectively.

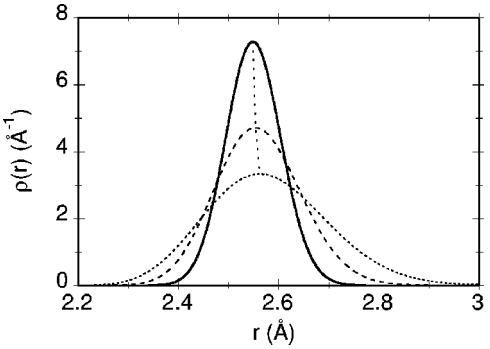

FIG. 13. Real distributions of first-shell interatomic distances reconstructed from EXAFS cumulants at 4, 250, and 500 K (continuous, dashed and dotted lines, respectively). The dotted vertical line evidences the positive shift of the maximum of the distributions, corresponding to the potential minimum, when temperature increases.

MSRDs should be interpreted by the same Debye temperature, and the ratio γ should be 2. The experimental value of γ for the first shell of copper depends on the choice of the mean free path λ (Fig. 12). It is in any case reasonable to assume that γ for the first shell of copper is larger than 2 and smaller than 3, indicating a slight parallel-perpendicular anisotropy. This experimental result is consistent with the high-temperature value $\gamma = 2.7$ recently obtained by PIMC Monte Carlo calculations.[38] A much higher value, $\gamma = 6$, was experimentally found for the first shell of germanium,[26] in agreement with model calculations for silicon[54] and satisfactorily reproduced by *ab initio* calculations.[55] The difference between copper and germanium can be attributed to the peculiar effect of optical modes in non-Bravais crystals.

Equations (15) and (17), connecting first and second cumulant to perpendicular and parallel MSRDs, respectively, are approximated. It has been shown in Ref. 14, through harmonic numerical simulations, that the approximation is very good for perfect parallel-perpendicular isotropy, and slightly worsens when the ratio γ and the degree of thermal disorder increases. For the first shell of copper, then, in view of the reduced anharmonicity and anisotropy ($\gamma < 3$), the high order corrections to Eqs. (15) and (17) can be considered negligible.

C. Effective potential

The good correspondence between temperature dependence of second, third, and fourth cumulants and their analytical expressions derived from the one-dimensional model[23] suggests that the shape of the effective EXAFS potential for the first shell of copper is insensitive to temperature within the experimental uncertainty.

The thermal expansion measured by the first EXAFS cumulant, δC_1^* (Fig. 5), is amenable to the sum of two contributions: the asymmetry of the effective potential, measured by the third cumulant (Fig. 7), and a rigid shift of the effective potential curve. It was shown in Ref. 14 that the harmonic thermal vibrations perpendicular to the bond direction, which are responsible for the difference $\delta C_1^* - \delta R_c$ between EXAFS and crystallographic thermal expansions, are connected to a rigid positive shift of the effective potential, but do not produce appreciable asymmetry of the distance distribution. In the case of parallel-perpendicular isotropy, $\gamma = 2$, the potential shift induced by perpendicular vibrations directly corresponds to the difference $\delta C_1^* - \delta R_c$. The further difference found between δR_c and δa (Fig. 7) suggests the presence of an additional positive potential shift, which was not observed in the case of germanium.[26] In other systems, a negative shift of the effective potential was instead observed.[25,29,30]

The relationship between anharmonicity of the crystal potential and asymmetry of the effective pair potential is far from trivial even for simple crystals like copper. As a consequence, it has been shown that no direct information on thermal expansion can be obtained from the third cumulant. In spite of this drawback, the cumulant method and the reference to an effective pair potential still present several advantages, which can be relevant when studying systems with a moderate degree of disorder, for which the cumulant series is fastly convergent (the limitations of the cumulant method for highly disordered systems have been discussed in Ref. 33). The cumulant analysis does not require to previously hypothesize the analytical form of a model distribution of distances; the distribution can instead be *a posteriori* reconstructed from the cumulants (see Fig. 13). The possibility of evaluating the effects of anharmonicity in a parametric form, through the values of the third and higher order cumulants, allows a more effective and accurate comparison with theoretical results than would be possible by directly comparing distributions. Besides, it is possible to subtract the effects of effective potential anharmonicity from the second cumulant, and evaluate the purely harmonic contribution to the parallel MSRD, which can be easily compared with harmonic force constant models.

The effective potential should not be confused with the interaction potential, since it depends on the averaged behavior of all the atoms in the crystal. Its use, eliminating the canonical temperature dependence of the distribution of distances, allows emphasizing the residual temperature dependence, which can be connected to more subtle physical effects. As a matter of fact, the negative shift experimentally observed in AgI (Ref. 25) has stimulated the development of a theoretical model which explains the shift in terms of the high mobility of Ag cations.[56]

VII. CONCLUSIONS

In this work, an EXAFS study of copper in the temperature interval from 4 to 500 K has been presented. No significant differences have been found between the relative values of cumulants obtained through a purely phenomenological analysis based on the *ratio method* (when applicable, say for the first coordination shell) and an analysis based on theoretical simulations (FEFF code).

Accurate values of the parallel MSRD have been obtained for the first four coordination shells. A slight but significant deviation from a perfectly isotropic Debye behavior has been detected, consisting in a weaker correlation and stronger anharmonicity effect for the second shell with respect to the other ones, in agreement with refined dynamical calculations. This result evidences the still unexplored potential of EXAFS for the study of subtle dynamical effects.

An accurate evaluation of odd cumulants was possible only for the first shell. The thermal expansion measured by the first cumulant is larger than the crystallographic thermal expansion. The difference has allowed an evaluation of the perpendicular MSRD with a good accuracy. The Debye temperature of the perpendicular MSRD is slightly larger than the one of the parallel MSRD, indicating a weak perpendicular-parallel anisotropy, in agreement with path-integral Monte Carlo calculations. Third and fourth cumulants have been satisfactorily fitted to equations derived from perturbative quantum calculations. The so obtained third and fourth order force constants of the effective pair potential allowed us to evaluate the anharmonic correction to the parallel MSRD, which amounts to less than 1.5 percent. The thermal expansion calculated from the third cumulant, due solely to the asymmetry of the effective pair potential, is non-negligibly smaller than the crystallographic one. The third cumulant cannot be neglected in the data analysis, if accurate values of the first cumulant are sought, but cannot be directly used to estimate the thermal expansion.

The regular temperature dependence of experimental cumulants, the agreement with quantum perturbative models and the overall consistency of results demonstrate the effectiveness of the cumulant expansion approach for the study of moderately disordered systems.

The good reproduction of the second and higher order cumulants within the framework of the one-dimensional model indicates that the shape of the effective pair potential is independent of temperature. The differences between the thermal expansions measured by the first and third cumulant as well as the crystallographic thermal expansion have been interpreted in terms of a rigid positive shift of the effective potential, which is only partially due to the relative motion perpendicular to the bond direction.

The results presented in this paper should contribute to a deeper understanding of the meaning of EXAFS parameters, and stimulate further efforts to increase the accuracy of EXAFS experiments and data analyses. Besides, they point to the still little explored possibilities of obtaining original information on local dynamical properties of solids. The calibration of these possibilities on simple crystalline systems like copper open new perspectives for studies of crystals with negative thermal expansion and of noncrystalline systems.

ACKNOWLEDGMENTS

The authors are grateful to C. Armellini and R. Graziola, as well as to the staff of the BM08-Gilda beamline at ESRF, for technical assistance, to J. Purans for stimulating discussions, and to T. Yokoyama for helpful advice. This work has been partially supported by the INFM project BM08-01-290.

*E-mail: fornasin@science.unitn.it

[1] T. M. Hayes and J. B. Boyce, Solid State Phys. **37**, 173 (1982).
[2] J. Rehr and R. Albers, Rev. Mod. Phys. **72**, 621 (2000).
[3] G. Beni and P. M. Platzman, Phys. Rev. B **14**, 1514 (1976).
[4] E. Sevillano, H. Meuth, and J. J. Rehr, Phys. Rev. B **20**, 4908 (1979).
[5] G. Dalba and P. Fornasini, J. Synchrotron Radiat. **4**, 243 (1997).
[6] P. Eisenberger and G. S. Brown, Solid State Commun. **29**, 481 (1979).
[7] J. B. Boyce, T. M. Hayes, and J. C. Mikkelsen, Jr., Phys. Rev. B **23**, 2876 (1981).
[8] J. M. Tranquada and R. Ingalls, Phys. Rev. B **28**, 3520 (1983).
[9] G. Dalba, P. Fornasini, M. Grazioli, and F. Rocca, Phys. Rev. B **52**, 11034 (1995).
[10] G. Dalba, D. Diop, P. Fornasini, and F. Rocca, J. Phys.: Condens. Matter **6**, 3599 (1994).
[11] G. Bunker, Nucl. Instrum. Methods Phys. Res. **207**, 437 (1983).
[12] E. D. Crozier, J. J. Rehr, and R. Ingalls, in *X-ray Absorption*, edited by D. C. Koningsberger and R. Prins (Wiley, New York, 1988), Chap. 9, pp. 373–442.
[13] P. Fornasini, J. Phys.: Condens. Matter **13**, 7859 (2001).
[14] P. Fornasini, F. Monti, and A. Sanson, J. Synchrotron Radiat. **8**, 1214 (2001).
[15] G. Dalba, P. Fornasini, and F. Rocca, Phys. Rev. B **47**, 8502 (1993).
[16] T. Yokoyama, T. Ohta, and H. Sato, Phys. Rev. B **55**, 11320 (1997).
[17] A. I. Frenkel and J. J. Rehr, Phys. Rev. B **48**, 585 (1993).
[18] T. Miyanaga and T. Fujikawa, J. Phys. Soc. Jpn. **63**, 1036 (1994).
[19] N. Van Hung and J. J. Rehr, Phys. Rev. B **56**, 43 (1997).
[20] T. Yokoyama, Phys. Rev. B **57**, 3423 (1998).
[21] H. Katsumata, T. Miyanaga, T. Yokoyama, T. Fujikawa, and T. Ohta, J. Synchrotron Radiat. **8**, 226 (2001).
[22] E. A. Stern, P. Livins, and Z. Zhang, Phys. Rev. B **43**, 8850 (1991).
[23] T. Yokoyama, J. Synchrotron Radiat. **6**, 323 (1999).
[24] L. Tröger, T. Yokoyama, D. Arvanitis, T. Lederer, M. Tischer, and K. Baberschke, Phys. Rev. B **49**, 888 (1994).
[25] G. Dalba, P. Fornasini, R. Gotter, and F. Rocca, Phys. Rev. B **52**, 149 (1995).
[26] G. Dalba, P. Fornasini, R. Grisenti, and J. Purans, Phys. Rev. Lett. **82**, 4240 (1999).

[27] B. T. M. Willis and A. W. Pryor, *Thermal Vibrations in Crystallography* (Cambridge University Press, Cambridge, 1975).
[28] T. Ishii, J. Phys.: Condens. Matter **4**, 8029 (1992).
[29] O. Kamishima, T. Ishii, H. Maeda, and S. Kashino, Solid State Commun. **103**, 141 (1997).
[30] G. Dalba, P. Fornasini, R. Grisenti, D. Pasqualini, D. Diop, and F. Monti, Phys. Rev. B **58**, 4793 (1998).
[31] S. a Beccara, G. Dalba, P. Fornasini, R. Grisenti, A. Sanson, and F. Rocca, Phys. Rev. Lett. **89**, 025503 (2002).
[32] J. Freund, Phys. Lett. A **157**, 256 (1991).
[33] A. Filipponi, J. Phys.: Condens. Matter **13**, R1 (2001).
[34] W. Böhmer and P. Rabe, J. Phys. C **12**, 2465 (1979).
[35] R. B. Greegor and F. W. Lytle, Phys. Rev. B **20**, 4902 (1979).
[36] E. A. Stern, B. A. Bunker, and S. M. Heald, Phys. Rev. B **21**, 5521 (1980).
[37] T. Yokoyama, T. Satsukawa, and T. Ohta, Jpn. J. Appl. Phys., Part 1 **28**, 1905 (1989).
[38] S. a Beccara, G. Dalba, P. Fornasini, R. Grisenti, F. Pederiva, A. Sanson, D. Diop, and F. Rocca, Phys. Rev. B **68**, 140301 (2003).
[39] J. Freund, R. Ingalls, and E. D. Crozier, Phys. Rev. B **39**, 12537 (1989).
[40] R. P. Feynman, *Statistical Mechanics* (Benjamin, Reading, MA, 1972).
[41] T. Yokoyama (private communication).
[42] T. Yokoyama, K. Kobayashi, T. Ohta, and A. Ugawa, Phys. Rev. B **53**, 6111 (1996).
[43] A. Ankudinov, B. Ravel, J. Rehr, and S. Conradson, Phys. Rev. B **58**, 7565 (1998).
[44] M. Newville, B. Ravel, J. Rehr, E. Stern, and Y. Yacoby, Physica B **208-209**, 154 (1995).
[45] Y. S. Touloukian, R. K. Kirby, R. E. Taylor, and P. D. Desai, *Thermophysical Properties of Matter* (Plenum, New York, 1977), Vol. 13.
[46] A. Bryan Edwards, D. J. Tildesley, and N. Binsted, Mol. Phys. **91**, 357 (1997).
[47] C. J. Martin and D. A. O'Connor, J. Phys. C **10**, 3521 (1977).
[48] J. T. Day, J. G. Mullen, and R. Shukla, Phys. Rev. B **52**, 168 (1995).
[49] G. K. White, Contemp. Phys. **193**, 34 (1993).
[50] V. Heine, P. R. L. Welche, and M. T. Dove, J. Am. Ceram. Soc. **82**, 1793 (1999).
[51] M. G. Tucker, M. T. Dove, and D. A. Keen, J. Phys.: Condens. Matter **12**, L425 (2000).
[52] F. H. Herbstein, Adv. Phys. **10**, 313 (1961).
[53] I. K. Jeong, R. H. Heffner, M. J. Graf, and S. J. L. Billinge, Phys. Rev. B **67**, 104301 (2003).
[54] O. H. Nielsen and W. Weber, J. Phys. C **13**, 2449 (1980).
[55] G. Birner, D. Strauch, and P. Pavone (private communication).
[56] T. Ishii, J. Phys. Soc. Jpn. **70**, 159 (2001).